

This work was written as part of one of the author's official duties as an Employee of the United States Government and is therefore a work of the United States Government. In accordance with 17 U.S.C. 105, no copyright protection is available for such works under U.S. Law.

Public Domain Mark 1.0

<https://creativecommons.org/publicdomain/mark/1.0/>

Access to this work was provided by the University of Maryland, Baltimore County (UMBC) ScholarWorks@UMBC digital repository on the Maryland Shared Open Access (MD-SOAR) platform.

Please provide feedback

Please support the ScholarWorks@UMBC repository by emailing scholarworks-group@umbc.edu and telling us what having access to this work means to you and why it's important to you. Thank you.

When the Milky Way hosted a quasar

Frédéric Marin^{1*}, Eugene Churazov^{2,3}, Ildar
 Khabibullin^{4,2,3}, Riccardo Ferrazzoli⁵, Laura
 Di Gesu⁶, Thibault Barnouin¹, Alessandro Di
 Marco⁵, Riccardo Middei^{7,8}, Alexey Vikhlinin^{9,3}, Enrico
 Costa⁵, Paolo Soffitta⁵, Fabio Muleri⁵, Rashid
 Sunyaev^{2,3}, William Forman⁹, Ralph Kraft⁹, Stefano
 Bianchi¹⁰, Immacolata Donnarumma⁶, Pierre-Olivier
 Petrucci¹¹, Teruaki Enoto¹², Iván Agudo¹³, Lucio A.
 Antonelli^{8,7}, Matteo Bachetti¹⁴, Luca Baldini^{15,16}, Wayne H.
 Baumgartner¹⁷, Ronaldo Bellazzini¹⁵, Stephen D.
 Bongiorno¹⁷, Raffaella Bonino^{18,19}, Alessandro
 Brez¹⁵, Niccolò Bucciantini^{20,21,22}, Fiamma
 Capitanio⁵, Simone Castellano¹⁵, Elisabetta
 Cavazzuti⁶, Chien-Ting Chen²³, Stefano
 Ciprini^{24,7}, Alessandra De Rosa⁵, Ettore Del Monte⁵, Niccolò
 Di Lalla²⁵, Victor Doroshenko²⁶, Michal Dovčiak²⁷, Steven R.
 Ehlert¹⁷, Yuri Evangelista⁵, Sergio Fabiani⁵, Javier A.
 Garcia²⁸, Shuichi Gunji²⁹, Kiyoshi Hayashida³⁰, Jeremy
 Heyl³¹, Adam Ingram³², Wataru Iwakiri^{33,34}, Svetlana G.
 Jorstad^{35,36}, Philip Kaaret³⁷, Vladimir Karas²⁷, Takao
 Kitaguchi¹², Jeffery J. Kolodziejczak¹⁷, Henric
 Krawczynski³⁸, Fabio La Monaca⁵, Luca Latronico¹⁸, Ioannis
 Liodakis³⁹, Simone Maldera¹⁸, Alberto Manfreda¹⁵, Andrea
 Marinucci⁶, Alan P. Marscher³⁵, Herman L.
 Marshall⁴⁰, Francesco Massaro^{18,19}, Giorgio Matt¹⁰, Ikuyuki
 Mitsuishi⁴¹, Tsunefumi Mizuno⁴², Michela Negro^{43,44,45}, C.-Y.
 Ng⁴⁶, Stephen L. O'Dell¹⁷, Nicola Omodei²⁵, Chiara
 Oppedisano¹⁸, Alessandro Papitto⁸, George G. Pavlov⁴⁷, Abel
 L. Peirson²⁵, Matteo Perri^{7,8}, Melissa Pesce-Rollins¹⁵, Maura
 Pilia¹⁴, Andrea Possenti¹⁴, Juri Poutanen⁴⁸, Simonetta
 Puccetti⁷, Brian D. Ramsey¹⁷, John Rankin⁵, Ajay

Ratheesh⁵, Oliver J. Roberts²³, Roger W. Romani²⁵, Carmelo Sgrò¹⁵, Patrick Slane⁹, Gloria Spandre¹⁵, Doug Swartz²³, Toru Tamagawa¹², Fabrizio Tavecchio⁴⁹, Roberto Taverna⁵⁰, Yuzuru Tawara⁴¹, Allyn F. Tennant¹⁷, Nicholas E. Thomas¹⁷, Francesco Tombesi^{51,24,52}, Alessio Trois¹⁴, Sergey S. Tsygankov⁴⁸, Roberto Turolla^{50,53}, Jacco Vink⁵⁴, Martin C. Weisskopf¹⁷, Kinwah Wu⁵³, Fei Xie,⁵ and Silvia Zane⁵³

¹Université de Strasbourg, CNRS, Observatoire Astronomique de Strasbourg, UMR 7550, 67000 Strasbourg, France.

²Max Planck Institute for Astrophysics,

Karl-Schwarzschild-Strasse 1, 85741 Garching, Germany.

³Space Research Institute of the Russian Academy of Sciences, Profsoyuznaya Str. 84/32, Moscow 117997, Russia.

⁴Universitäts-Sternwarte, Fakultät für Physik,

Ludwig-Maximilians-Universität München, Scheinerstr.1, 81679 München, Germany.

⁵INAF Istituto di Astrofisica e Planetologia Spaziali, Via del Fosso del Cavaliere 100, 00133 Roma, Italy.

⁶ASI - Agenzia Spaziale Italiana, Via del Politecnico snc, 00133 Roma, Italy.

⁷Space Science Data Center, Agenzia Spaziale Italiana, Via del Politecnico snc, 00133 Roma, Italy.

⁸INAF Osservatorio Astronomico di Roma, Via Frascati 33, 00078 Monte Porzio Catone (RM), Italy.

⁹Center for Astrophysics, Harvard & Smithsonian, 60 Garden St, Cambridge, MA 02138, USA.

¹⁰Dipartimento di Matematica e Fisica, Università degli Studi Roma Tre, Via della Vasca Navale 84, 00146 Roma, Italy.

¹¹Université Grenoble Alpes, CNRS, IPAG, 38000 Grenoble, France.

¹²RIKEN Cluster for Pioneering Research, 2-1 Hirosawa, Wako, Saitama 351-0198, Japan.

¹³Instituto de Astrofísica de Andalucía—CSIC, Glorieta de la Astronomía s/n, 18008 Granada, Spain.

¹⁴INAF Osservatorio Astronomico di Cagliari, Via della Scienza 5, 09047 Selargius (CA), Italy.

¹⁵Istituto Nazionale di Fisica Nucleare, Sezione di Pisa, Largo B. Pontecorvo 3, 56127 Pisa, Italy.

- ¹⁶Dipartimento di Fisica, Università di Pisa, Largo B. Pontecorvo 3, 56127 Pisa, Italy.
- ¹⁷NASA Marshall Space Flight Center, Huntsville, AL 35812, USA.
- ¹⁸Istituto Nazionale di Fisica Nucleare, Sezione di Torino, Via Pietro Giuria 1, 10125 Torino, Italy.
- ¹⁹Dipartimento di Fisica, Università degli Studi di Torino, Via Pietro Giuria 1, 10125 Torino, Italy.
- ²⁰INAF Osservatorio Astrofisico di Arcetri, Largo Enrico Fermi 5, 50125 Firenze, Italy.
- ²¹Dipartimento di Fisica e Astronomia, Università degli Studi di Firenze, Via Sansone 1, 50019 Sesto Fiorentino (FI), Italy.
- ²²Istituto Nazionale di Fisica Nucleare, Sezione di Firenze, Via Sansone 1, 50019 Sesto Fiorentino (FI), Italy.
- ²³Science and Technology Institute, Universities Space Research Association, Huntsville, AL 35805, USA.
- ²⁴Istituto Nazionale di Fisica Nucleare, Sezione di Roma “Tor Vergata”, Via della Ricerca Scientifica 1, 00133 Roma, Italy.
- ²⁵Department of Physics and Kavli Institute for Particle Astrophysics and Cosmology, Stanford University, Stanford, California 94305, USA.
- ²⁶Institut für Astronomie und Astrophysik, Universität Tübingen, Sand 1, 72076 Tübingen, Germany.
- ²⁷Astronomical Institute of the Czech Academy of Sciences, Boční II 1401/1, 14100 Praha 4, Czech Republic.
- ²⁸California Institute of Technology, Pasadena, CA 91125, USA.
- ²⁹Yamagata University, 1-4-12 Kojirakawa-machi, Yamagata-shi 990-8560, Japan.
- ³⁰Osaka University, 1-1 Yamadaoka, Suita, Osaka 565-0871, Japan.
- ³¹University of British Columbia, Vancouver, BC V6T 1Z4, Canada.
- ³²School of Mathematics, Statistics and Physics, Newcastle University, Herschel Building, Newcastle upon Tyne, NE1 7RU, UK.
- ³³Department of Physics, Faculty of Science and Engineering, Chuo University, 1-13-27 Kasuga, Bunkyo-ku, Tokyo 112-8551, Japan.
- ³⁴International Center for Hadron Astrophysics, Chiba University, Chiba 263-8522, Japan.

- ³⁵Institute for Astrophysical Research, Boston University, 725 Commonwealth Avenue, Boston, MA 02215, USA.
- ³⁶Department of Astrophysics, St. Petersburg State University, Universitetsky pr. 28, Petrodvoretz, 198504 St. Petersburg, Russia.
- ³⁷Department of Physics and Astronomy, University of Iowa, Iowa City, IA 52242, USA.
- ³⁸Physics Department and McDonnell Center for the Space Sciences, Washington University in St. Louis, St. Louis, MO 63130, USA.
- ³⁹Finnish Centre for Astronomy with ESO, 20014 University of Turku, Finland.
- ⁴⁰MIT Kavli Institute for Astrophysics and Space Research, Massachusetts Institute of Technology, 77 Massachusetts Avenue, Cambridge, MA 02139, USA.
- ⁴¹Graduate School of Science, Division of Particle and Astrophysical Science, Nagoya University, Furo-cho, Chikusa-ku, Nagoya, Aichi 464-8602, Japan.
- ⁴²Hiroshima Astrophysical Science Center, Hiroshima University, 1-3-1 Kagamiyama, Higashi-Hiroshima, Hiroshima 739-8526, Japan.
- ⁴³University of Maryland, Baltimore County, Baltimore, MD 21250, USA.
- ⁴⁴NASA Goddard Space Flight Center, Greenbelt, MD 20771, USA.
- ⁴⁵Center for Research and Exploration in Space Science and Technology, NASA/GSFC, Greenbelt, MD 20771, USA.
- ⁴⁶Department of Physics, The University of Hong Kong, Pokfulam, Hong Kong.
- ⁴⁷Department of Astronomy and Astrophysics, Pennsylvania State University, University Park, PA 16802, USA.
- ⁴⁸Department of Physics and Astronomy, 20014 University of Turku, Finland.
- ⁴⁹INAF Osservatorio Astronomico di Brera, Via E. Bianchi 46, 23807 Merate (LC), Italy.
- ⁵⁰Dipartimento di Fisica e Astronomia, Università degli Studi di Padova, Via Marzolo 8, 35131 Padova, Italy.
- ⁵¹Dipartimento di Fisica, Università degli Studi di Roma “Tor Vergata”, Via della Ricerca Scientifica 1, 00133 Roma, Italy.

⁵²Department of Astronomy, University of Maryland, College Park, Maryland 20742, USA.

⁵³Mullard Space Science Laboratory, University College London, Holmbury St Mary, Dorking, Surrey RH5 6NT, UK.

⁵⁴Anton Pannekoek Institute for Astronomy & GRAPPA, University of Amsterdam, Science Park 904, 1098 XH Amsterdam, The Netherlands.

⁵⁵Guangxi Key Laboratory for Relativistic Astrophysics, School of Physical Science and Technology, Guangxi University, Nanning 530004, China.

*Corresponding author(s). E-mail(s):
frederic.marin@astro.unistra.fr;

Abstract

The Galactic Center harbors diffuse X-ray emission co-spatial with giant molecular clouds and featuring hard X-ray spectra with a prominent fluorescent iron line at 6.4 keV [1–3]. These spectral properties are characteristic of the reflected emission from a neutral gas illuminated by X-rays. However, there are no persistent X-ray sources in that region that are bright enough to provide the required illumination level. Moreover, the observed diffuse emission is variable on time scales of years [4, 5], implying that the primary source of X-rays must be variable, too. The most exciting and far-reaching scenario is that a very powerful flare from the central supermassive black hole of the Milky Way, Sgr A*, provided the required flux of X-ray photons, when for a period shorter than a few years it became at least five orders of magnitude brighter than is typically observed today. Even if the primary emission was unpolarized, the reflected emission should be polarized in the direction perpendicular to the scattering plane with the degree of polarization being set by the scattering angle. Therefore, by measuring X-ray polarization one can infer the direction towards the primary source and, simultaneously, the mutual positions in space of the source and the cloud [6]. Here, we report the detection of X-ray polarization from the Galactic Center region obtained by the recently launched Imaging X-ray Polarimetry Explorer (IXPE) mission. For a large region where Chandra and XMM-Newton identify spectral signatures of the reflection, IXPE measures a polarization degree of $31\% \pm 11\%$ with a polarization angle $-48^\circ \pm 11^\circ$ for the scattered continuum. The latter corroborates the conjecture that Sgr A* is the primary source of illuminating photons, while the former implies that some 200 years ago our Galactic Center hosted an extremely bright active galactic nucleus, on par with the ones found in Seyfert galaxies, though only for a short time.

Keywords: polarization, black holes, quasars, Galactic center

According to the current paradigm supported by observations and numerical simulations, every massive galaxy hosts a supermassive black hole in its center [7]. However, only a small fraction of these black holes (less than 10%) in the nearby Universe appears as bright active galactic nuclei (AGN) with luminosity at a sizable fraction of the Eddington luminosity. The Milky Way Galaxy follows both trends: it has a ~ 4 million solar mass black hole (known as Sgr A*, [8, 9]) with a typical luminosity some 6–8 orders of magnitude below the Eddington level [10]. This is what we observe today.

Thanks to the time-delay caused by finite light propagation speed, one can hope to glimpse into the past of supermassive black hole (SMBH) activity by observing ‘echoes’ of the brightest episodes arising due to reflection of the primary radiation on the dense interstellar medium ubiquitous in the innermost region of the Galaxy. As the size of this region, called the Central Molecular Zone, amounts to hundreds of light years, this also sets the maximum age we can look back in time using this technique to $\lesssim 1000$ years.

Indeed, the first maps of the hard X-ray (8.5–22 keV) emission from the Galactic Center region [1, 2] exhibited spatial correlation with the distribution of dense molecular gas, and in particular with the most massive Giant Molecular Complexes (GMC), e.g. Sgr B2. Later on, spectroscopic X-ray observations of these GMCs have revealed fluorescent line emission of neutral/weakly-ionized iron, a power-law spectrum and a reflection continuum extending from a few keV to a hundred keV [3, 11–13], both being characteristic of X-ray reflection from cold gas. Although a similar spectrum might also be produced by interaction of cosmic rays with the molecular gas, the diffuse emission appeared to be variable on time scales comparable with the light-crossing time for its apparent extent, clearly favoring the X-ray illumination scenario with a correspondingly variable primary source [4, 5]. Variability of the most compact reflecting regions puts a stringent upper limit on the duration of the primary flare, $\lesssim 1.6$ yr [14].

Since Compton scattering is responsible for the reflection of X-ray continuum photons, the X-ray emission coming from molecular clouds (excluding fluorescent lines) should be polarized in the direction perpendicular to the scattering plane with the degree of polarization being set by the scattering angle. This provides an independent way of finding the position of the primary source of X-rays (conjectured to be Sgr A*) relative to the scattering clouds both in the sky plane and along the line of sight [6, 15, 16]. If confirmed, this would mean that Sgr A* indeed was similar to a low-luminosity quasar [17, 18] with an X-ray luminosity $\sim 10^{40}$ erg s $^{-1}$ a few hundred years ago.

The recent launch of the first imaging X-ray polarimetry mission IXPE [19] offered a perfect opportunity to check this prediction by observing the molecular complex Sgr A, which is currently the brightest one in reflected X-ray emission [20]. The Sgr A region (centered on Right Ascension 266.51° and Declination -28.89° in equatorial coordinates) was observed by IXPE in 2022 with a total integration time amounting to 0.93 megaseconds (324 kiloseconds from February 27 to March 6, and 639 kiloseconds from March 10 to March 24),

after filtering for episodes of enhanced instrumental background. In addition to the X-ray polarimetric data, a few quasi-simultaneous observations with the Chandra X-ray observatory were acquired from February 26 to March 11, 2022 using the ACIS-I detector (OBSIDs 24373, 24820, and 26353), which covers the 0.3–10.0 keV band with a spectral resolution of $\Delta E \sim 0.3$ keV near $E = 6$ keV and arcsecond angular resolution. The Chandra data were used to identify regions where the reflected emission is strong and to extract spectra from these regions.

The comparison of the X-ray (4–8 keV) surface brightness maps of the Galactic Center region obtained by Chandra and IXPE (angular resolution $< 30''$) is shown in Fig. 1 (technical details about the data reduction of the IXPE and Chandra observations are described in the Methods section). We excluded the 2–4 keV band as it is entirely dominated by unpolarized plasma emission [21–23].

Based on the Chandra image only, we pre-selected a circular extraction region with a radius $4.5'$ centered on the Sgr A complex. This choice was driven by the desire to collect as many "reflected" photons as possible and, at the same time, avoid the very edges of the IXPE detectors. The selected region does include most of the areas where the reflection emission is elevated, but avoids regions affected by very bright sources that enter the IXPE field-of-view as a result of the pointing dithering pattern.

A bright $1'$ region associated with the non-thermal object G0.13-0.11 [24], see Fig. 1, was excluded to avoid possible contamination of the polarised signal. As shown in Fig. 2, the extracted IXPE spectrum shows a good correspondence with the Chandra data and with the data of archival XMM-Newton observations for the same region (see Methods). A bump, associated with the iron lines at 6.4 and 6.7 keV, is clearly seen, even with the lower spectral resolution of IXPE ($\Delta E \sim 0.5$ keV near $E = 2$ keV), and the spectral emission model based on XMM-Newton and Chandra data consistently well describes the spectrum obtained by IXPE, given the current level of cross-calibration uncertainties between the instruments.

The total model is built from several components that are detailed in the Methods section. All of them, except for the component representing the reflected emission from the molecular cloud, are assumed to be constant in time, i.e. staying the same for all three datasets. The reflected emission, in turn, consists of a combination of the Compton scattered and photo-absorbed continuum, and fluorescent emission lines, calculated self-consistently based on the Monte-Carlo calculations of the reflection spectrum [25]. Among all emission components, only the continuum part of the reflected spectrum is predicted to be polarized [16, 22, 26], so that the Stokes parameters Q and U of the emission measured by IXPE need to be related to the reflection continuum contribution $I_{\text{ref},c}$, and not to the total observed intensity I. Since in the simplest single-scattering scenario no dependence of polarization degree on photon energy is expected, the spectral shape of Q and U should resemble the shape of $I_{\text{ref},c}$.

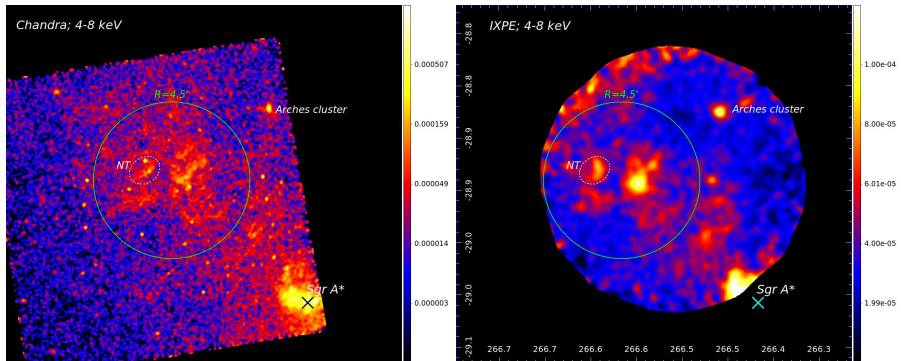


Fig. 1 Quasi-simultaneous Chandra (left) and IXPE (right) 4–8 keV X-ray surface brightness maps of the Galactic center region to the North-East from Sgr A*. The maps are in equatorial coordinates, North is up. The IXPE image is in units of counts $\text{s}^{-1} \text{ arcmin}^{-2} \text{ cm}^{-2}$ colour-coded on a linear scale (see the colorbar on the right). For IXPE, the edges of the image, where the exposure (including vignetting effects) drops below 15% of the maximal value, have been truncated. For Chandra, a logarithmic scale is used to show both diffuse and compact sources. The positions of the supermassive black hole Sgr A* and the Arches star cluster are labeled. The area where reflection emission is strong in the Chandra data is shown using a green $4.5'$ radius circle. This circle was used to extract I, Q, and U spectra from the IXPE data. The same region was used for Chandra and XMM-Newton spectral analysis. The white dashed ellipse shows the location of a bright non-thermal (NT) source G0.13-0.11 [24] that was masked for the spectra extraction.

The observed spectra of Stokes parameters Q and U are shown in Fig. 3. The Q values are close to zero, while U is mostly negative, suggesting a polarization angle close to -45° . The best-fitting reflection model to the observed Q and U spectra is shown with the solid lines. Here, we have explicitly assumed that all emission from the entire region has the same polarisation degree and angle, which is valid if a compact (in 3D) group of clouds is illuminated. With these simplifying assumptions, our model has only two free parameters that were derived from the IXPE data: a degree of polarization $P = 31 \pm 11\%$ and a polarisation angle $\phi = -48^\circ \pm 11^\circ$ with the error bars given at 68% confidence level (see Fig. 4). For comparison, the dashed lines in Fig. 3 show the expected Q and U spectra for the same ϕ but for a 100% polarized reflected component. As explained in Methods, the uncertainty in the absolute normalization of the reflected component is $\sim 30\%$. Therefore, the constraints on the polarization degree could be written as a multiplicative combination of statistical and systematic uncertainties: $P = (31 \pm 11)_{\text{stat.}} \% \times (1.0 \pm 0.3)_{\text{syst.}}$. Even with this extra uncertainty in P , it is clear that the observed polarization degree is significantly smaller than 100%. At the same time, this systematic uncertainty does not affect the significance of the polarized signal detection, i.e. $P > 0$, which corresponds to ≈ 3 standard deviations.

The measured polarization angle ϕ , which in the IAU convention is counted in the anti-clockwise direction from North in the equatorial coordinate system, is consistent with the hypothesis that Sgr A* is the primary source. Indeed, for a cloud located at the center of our spectrum extraction region, the line

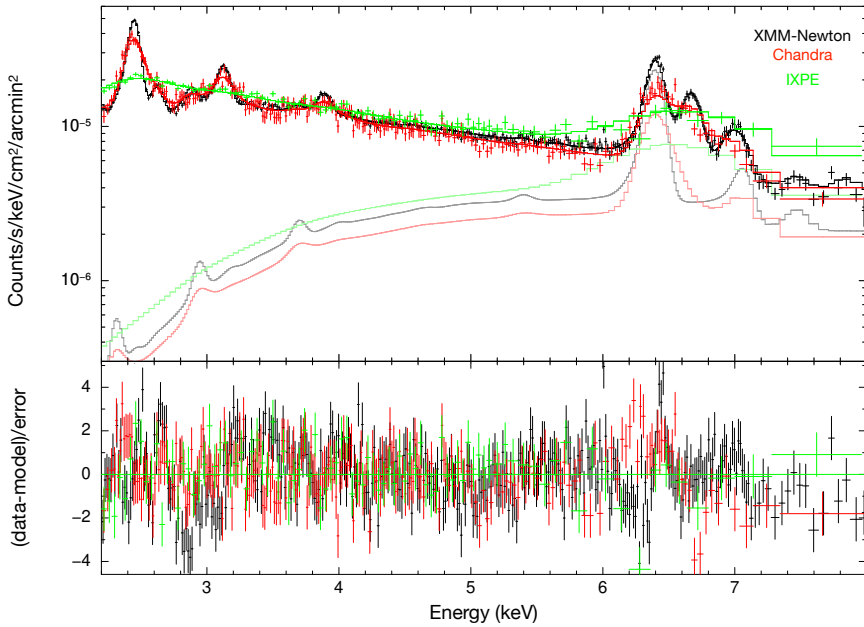


Fig. 2 Top panel: Spectra of the X-ray emission extracted from the circular region shown in Fig. 1 in the data of Chandra (red), IXPE (green) and archival XMM-Newton (black) observations, after division by energy-dependent effective area of each telescope. The solid lines correspond to the best-fitting models convolved with the spectral responses of the telescopes resulting in strong smearing of the emission lines in the IXPE data. Parameters of the stationary emission components were fixed among all three datasets, and only normalization of the reflection component was allowed to vary between them. Faint lines show contribution of the reflected component to the combined model (see Methods for individual description of each component). As demonstrated by the residuals shown in the bottom panel, the model provides a good fit for the soft part of the spectra for all three datasets, while contributions of the time-variable reflection component in the quasi-simultaneous Chandra and IXPE observations are consistent with each other, given the current level of cross-calibration uncertainties.

orthogonal to the direction towards Sgr A* corresponds to $\phi = -42^\circ$. Since this is close to the best-fitting value of $\phi = -48^\circ$, fixing it to -42° does not affect the errors on the degree polarisation, in agreement with expectations.

The degree of polarisation P of the reflected continuum is directly related to the scattering angle θ in the single scattering approximation, i.e. $P = (1 - \mu^2)/(1 + \mu^2)$, where $\mu = \cos \theta$. For any given value of P , if θ is a solution, then $\pi - \theta$ is a solution too. For $P = 31 \pm 11\%$, these two solutions are 43_{-8}^{+7} and 137_{-8}^{+7} degrees, respectively. A similar level of uncertainties is caused by the $\sim 30\%$ systematic error in the value of P . These scattering angles in turn fix the geometry of the problem, i.e. the line-of-sight position of the scattering cloud with respect to the primary source (see Methods).

For a given scattering angle θ , one can also calculate the age of the flare t_{flare} , i.e. a time delay associated with the propagation of X-ray photons from the primary source to the cloud and then to the observer. Adopting a projected distance between Sgr A* and the scattering clouds of 25 pc, i.e. the distance

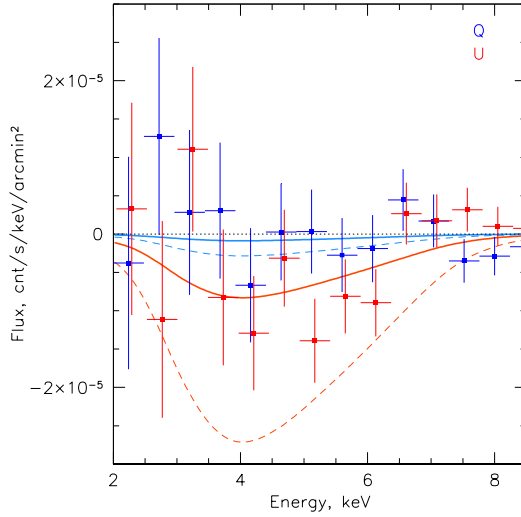


Fig. 3 Stokes parameters Q (blue) and U (red) spectra extracted from the circular region shown in Fig. 2. For clarity, both the Q and U data points are slightly shifted in energy. The solid blue and red lines represent the best fitting reflection model (the Compton-scattered continuum component only) to the Q and U spectra with a degree of polarization 31% and the polarization angle -48° . The model has been convolved with the IXPE spectral response. The thinner dashed lines are representative of the maximum Q and U that one could expect for 90° scattering that would lead to a 100% polarized reflected continuum.

between the SMBH and the center of our extraction zone in the sky plane, the two solutions for θ translate into two t_{flare} values: 33^{+6}_{-7} and 205^{+30}_{-50} years, respectively. Once again, the systematic uncertainties are comparable to the quoted statistical errors (see Methods). From the point of view of polarization properties, both solutions are equivalent. However, the ‘older’ flare is far more plausible, given that (i) a cloud located behind Sgr A* will remain bright longer than the same cloud in front of it [27], and, therefore, on average, the chances to spot it in a bright phase are higher, and (ii) the “younger” flare from Sgr A* would have been observed directly. Indeed, the Advanced Satellite for Cosmology and Astrophysics (ASCA) was in orbit and active 30 years ago, and the GMCs were already bright at the time [3, 28], while Sgr A* was not. The Sgr B2 cloud, which in the sky plane is much further away from Sgr A* than the area covered by IXPE, was bright too. This fact strongly suggests that the flare was significantly older than 30 years, or that there were multiple flares. Here, the former scenario is adopted.

Existing observational data [25, 29], including those of IXPE, suggest the broad-band (1–100 keV) Sgr A* luminosity during the flare was in the range from a few 10^{39} to $\sim 10^{44}$ ergs $^{-1}$. The lower limit comes from the brightest levels of the surface brightness observed over years (see Methods), while the

upper limit corresponds to the Eddington-level luminosity of Sgr A*, which could be exceeded in some scenarios. In the former case, a 1–2 years-long flare is needed, while in the latter, an hour-long outburst might be sufficient, since the observational data better constrain the fluence of the flare (product of the luminosity and duration of the flare) $\Delta t \times L_X \sim$ a few 10^{47} erg, rather than its luminosity, with an additional constraint that $\Delta t < 1.6$ yr [29]. Looking at a landscape of possible classes of transient events [30] that can explain such parameters, one could mention Accretion Induced Collapse of white dwarfs, sub-luminous gamma-ray bursts, and Tidal Disruption Events. One could add a transient accretion event on Sgr A* (not directly related to a tidal disruption event) to this list, too. The second group of transients, which fall short a factor of 10–100 in terms of fluence, includes Giant Flares from Soft Gamma-ray Repeaters / Magnetars, Type II Supernova Breakouts, and major outbursts of Ultra-Luminous X-ray sources. The second line of reasoning could come from the comparison of the expected event rates, bearing in mind that the fluence was calculated for the adopted distance between the clouds and Sgr A*, and, therefore, the assumption that the source is further away would boost the required fluence. These considerations favor Sgr A* as the prime candidate, especially considering the consistency of its position with the measured polarization degree, although other scenarios are not completely eliminated. Thus, IXPE observations provide good support that a few hundred years ago our Galactic Center hosted a real AGN, though for a limited time.

The detection of a faint and diffuse source such as reflection from molecular clouds in the Galactic Center region remains a challenging exercise that requires very long observations. Current IXPE data demonstrate this goal is within the reach of IXPE, paving a way for future (even longer) observations of IXPE that can improve the statistical power of the data and allow for a more detailed analysis, including spatially resolved polarisation, to verify the single flare scenario and the determination of the intrinsic polarization of the flares to probe the origin of the radiation and constraints on the multiple-flare scenarios.

Acknowledgments. The Imaging X ray Polarimetry Explorer (IXPE) is a joint US and Italian mission. The US contribution is supported by the National Aeronautics and Space Administration (NASA) and led and managed by its Marshall Space Flight Center (MSFC), with industry partner Ball Aerospace (contract NNM15AA18C). The Italian contribution is supported by the Italian Space Agency (Agenzia Spaziale Italiana, ASI) through contract ASI-OHBI-2017-12-I.0, agreements ASI-INAF-2017-12-H0 and ASI-INFN-2017.13-H0, and its Space Science Data Center (SSDC) with agreements ASI-INAF-2022-14-HH.0 and ASI-INFN 2021-43-HH.0, and by the Istituto Nazionale di Astrofisica (INAF) and the Istituto Nazionale di Fisica Nucleare (INFN) in Italy. This research used data products provided by the IXPE Team (MSFC, SSDC, INAF, and INFN) and distributed with additional software tools by the High-Energy Astrophysics Science Archive Research Center (HEASARC), at NASA Goddard Space Flight Center (GSFC). F.M. is grateful

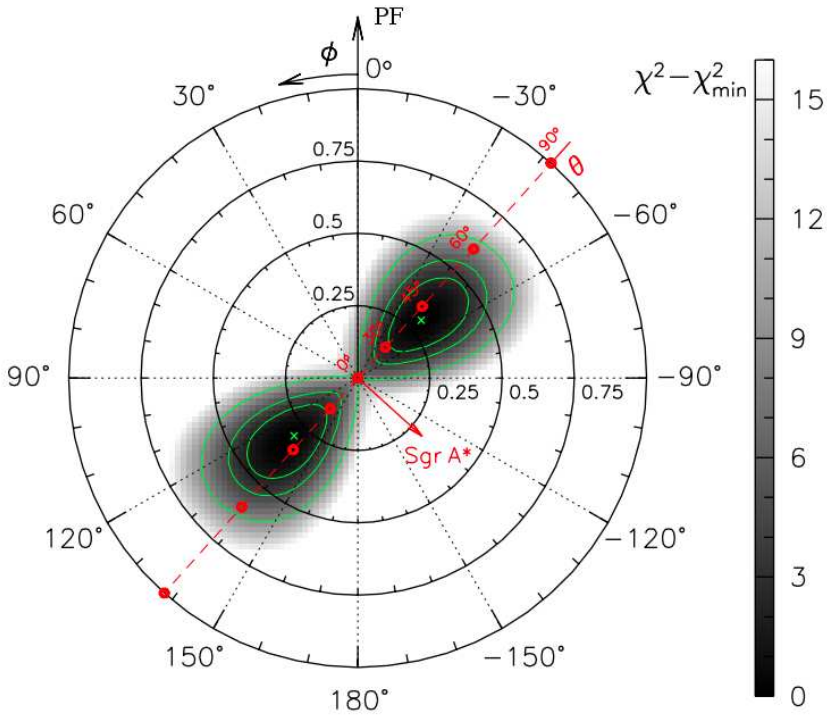


Fig. 4 Map of the $\chi^2 - \chi_{\min}^2$ statistic for the fit of the Stokes parameters Q and U spectra with the reflection continuum model in polar coordinates with radius equal to the polarization fraction (PF) and the azimuthal angle showing the position angle of the electric field vector (ϕ). The minimal value of the statistic χ_{\min}^2 corresponds to the best fitting values $\phi = -48^\circ$ and $P = 31\%$ (marked as green crosses), and the contours show 68, 90 and 99% confidence levels. The hypothesis that Sgr A* is the primary source of illuminating X-ray flux, implies the polarization angle $\phi = -42^\circ$ for the center of the region used for extraction of the Q and U spectra, as marked with the red dashed line. The circles on this line depict expected polarization degrees for the scattering angle changing from 0(180) to 30(150), 45(135), 60(120), and 90 degrees.

to the Astronomical observatory of Strasbourg, the CNRS and the University of Strasbourg under whose benevolence this paper was written. I.K. acknowledges support by the COMPLEX project from the European Research Council (ERC) under the European Union's Horizon 2020 research and innovation program grant agreement ERC-2019-AdG 882679. P.O.P. acknowledges financial support from the french National Program of High Energy (PNHE/CNRS) and from the french national space agency (Centre National d'Etudes Spatiales – CNES). A.I. acknowledges support from the Royal Society. A.V., W.F., and R.K. acknowledge support from NASA Grant GO1-22136X, the Smithsonian Institution, and the Chandra High Resolution Camera Project through NASA contract NAS8-03060. C.-Y. Ng is supported by a GRF grant of the Hong Kong Government under HKU 17305419.

Author contributions. F. Marin led the IXPE observation, contributed to the analysis and led the writing of the paper. E. Churazov, I. Khabibullin, R. Ferrazzoli, L. Di Gesu, T. Barnouin, A. Di Marco, R. Middei, E. Costa, P. Soffitta, F. Muleri and R. Sunyaev contributed to the IXPE analysis, discussion and writing of the paper. A. Vikhlinin, W. Forman and R. Kraft provided and reduced the Chandra data used in this paper. S. Bianchi, D. Immacolata, P.-O. Petrucci and T. Enoto contributed with discussion and parts of the paper. The remaining authors are part of the IXPE team whom significant contribution made the satellite and the Galactic center observation possible.

Competing interest. Authors declare that they have no competing interests.

Data availability. The IXPE data that support the findings of this study are freely available in the HEASARC IXPE Data Archive (<https://heasarc.gsfc.nasa.gov/docs/ixpe/archive/>). The XMM-Newton data can be found on the same website, while the Chandra data will be public after one year from the observation date.

Code availability. The analysis and simulation software *ixpeobssim* developed by IXPE collaboration and its documentation is available publicly through the web-page <https://ixpeobssim.readthedocs.io/en/latest/?badge=latest.494>. XSPEC is distributed and maintained under the aegis of the HEASARC and can be downloaded as part of HEASoft from <http://heasarc.gsfc.nasa.gov/docs/software/lheasoft/download.html>.

References

- [1] Sunyaev, R.A., Markevitch, M., Pavlinsky, M.: The Center of the Galaxy in the Recent Past: A View from GRANAT. *Astrophysical Journal* **407**, 606 (1993). <https://doi.org/10.1086/172542>
- [2] Markevitch, M., Sunyaev, R.A., Pavlinsky, M.: Two sources of diffuse X-ray emission from the Galactic Centre. *Nature* **364**(6432), 40–42 (1993). <https://doi.org/10.1038/364040a0>
- [3] Koyama, K., Maeda, Y., Sonobe, T., Takeshima, T., Tanaka, Y., Yamauchi, S.: ASCA View of Our Galactic Center: Remains of Past Activities in X-Rays? *Publications of the Astronomical Society of Japan* **48**, 249–255 (1996). <https://doi.org/10.1093/pasj/48.2.249>
- [4] Clavel, M., Terrier, R., Goldwurm, A., Morris, M.R., Ponti, G., Soldi, S., Trap, G.: Echoes of multiple outbursts of Sagittarius A* revealed by Chandra. *Astronomy and Astrophysics* **558**, 32 (2013) <https://arxiv.org/abs/1307.3954> [astro-ph.HE]. <https://doi.org/10.1051/0004-6361/201321667>

- [5] Terrier, R., Clavel, M., Soldi, S., Goldwurm, A., Ponti, G., Morris, M.R., Chuard, D.: An X-ray survey of the central molecular zone: Variability of the Fe K α emission line. *Astronomy and Astrophysics* **612**, 102 (2018) <https://arxiv.org/abs/1712.04232> [astro-ph.HE]. <https://doi.org/10.1051/0004-6361/201730837>
- [6] Churazov, E., Sunyaev, R., Sazonov, S.: Polarization of X-ray emission from the Sgr B2 cloud. *Monthly Notices of the Royal Astronomical Society* **330**(4), 817–820 (2002) <https://arxiv.org/abs/astro-ph/0111065> [astro-ph]. <https://doi.org/10.1046/j.1365-8711.2002.05113.x>
- [7] Kormendy, J., Ho, L.C.: Coevolution (Or Not) of Supermassive Black Holes and Host Galaxies. *ARA&A* **51**(1), 511–653 (2013) <https://arxiv.org/abs/1304.7762> [astro-ph.CO]. <https://doi.org/10.1146/annurev-astro-082708-101811>
- [8] GRAVITY Collaboration, Abuter, R., Amorim, A., Bauböck, M., Berger, J.P., Bonnet, H., Brandner, W., Cardoso, V., Clénet, Y., de Zeeuw, P.T., Dexter, J., Eckart, A., Eisenhauer, F., Förster Schreiber, N.M., Garcia, P., Gao, F., Gendron, E., Genzel, R., Gillessen, S., Habibi, M., Haubois, X., Henning, T., Hippler, S., Horrobin, M., Jiménez-Rosales, A., Jochum, L., Jocu, L., Kaufer, A., Kervella, P., Lacour, S., Lapeyrère, V., Le Bouquin, J.-B., Léna, P., Nowak, M., Ott, T., Paumard, T., Perraut, K., Perrin, G., Pfuhl, O., Rodríguez-Coira, G., Shangguan, J., Scheithauer, S., Stadler, J., Straub, O., Straubmeier, C., Sturm, E., Tacconi, L.J., Vincent, F., von Fellenberg, S., Waisberg, I., Widmann, F., Wieprecht, E., Wiezorrek, E., Woillez, J., Yazici, S., Zins, G.: Detection of the Schwarzschild precession in the orbit of the star S2 near the Galactic centre massive black hole. *Astronomy and Astrophysics* **636**, 5 (2020) <https://arxiv.org/abs/2004.07187> [astro-ph.GA]. <https://doi.org/10.1051/0004-6361/202037813>
- [9] Event Horizon Telescope Collaboration, Akiyama, K., Alberdi, A., Alef, W., Algaba, J.C., Anantua, R., Asada, K., Azulay, R., Bach, U., Baczko, A.-K., Ball, D., Baloković, M., Barrett, J., Bauböck, M., Benson, B.A., Bintley, D., Blackburn, L., Blundell, R., Bouman, K.L., Bower, G.C., Boyce, H., Bremer, M., Brinkerink, C.D., Brissenden, R., Britzen, S., Broderick, A.E., Brogiere, D., Bronzwaer, T., Bustamante, S., Byun, D.-Y., Carlstrom, J.E., Ceccobello, C., Chael, A., Chan, C.-k., Chatterjee, K., Chatterjee, S., Chen, M.-T., Chen, Y., Cheng, X., Cho, I., Christian, P., Conroy, N.S., Conway, J.E., Cordes, J.M., Crawford, T.M., Crew, G.B., Cruz-Osorio, A., Cui, Y., Davelaar, J., Laurentis, M.D., Deane, R., Dempsey, J., Desvignes, G., Dexter, J., Dhruv, V., Doeleman, S.S., Dougal, S., Dzib, S.A., Eatough, R.P., Emami, R., Falcke, H., Farah, J., Fish, V.L., Fomalont, E., Ford, H.A., Fraga-Encinas, R., Freeman, W.T., Friberg, P., Fromm, C.M., Fuentes, A., Galison, P., Gammie, C.F., García, R., Gentaz, O., Georgiev, B., Goddi, C., Gold, R., Gómez-Ruiz,

A.I., Gómez, J.L., Gu, M., Gurwell, M., Hada, K., Haggard, D., Haworth, K., Hecht, M.H., Hesper, R., Heumann, D., Ho, L.C., Ho, P., Honma, M., Huang, C.-W.L., Huang, L., Hughes, D.H., Ikeda, S., Impellizzeri, C.M.V., Inoue, M., Issaoun, S., James, D.J., Jannuzi, B.T., Janssen, M., Jeter, B., Jiang, W., Jiménez-Rosales, A., Johnson, M.D., Jorstad, S., Joshi, A.V., Jung, T., Karami, M., Karuppusamy, R., Kawashima, T., Keating, G.K., Kettenis, M., Kim, D.-J., Kim, J.-Y., Kim, J., Kim, J., Kino, M., Koay, J.Y., Kocherlakota, P., Kofuji, Y., Koch, P.M., Koyama, S., Kramer, C., Kramer, M., Krichbaum, T.P., Kuo, C.-Y., Bella, N.L., Lauer, T.R., Lee, D., Lee, S.-S., Leung, P.K., Levis, A., Li, Z., Lico, R., Lindahl, G., Lindqvist, M., Lisakov, M., Liu, J., Liu, K., Liuzzo, E., Lo, W.-P., Lobanov, A.P., Loinard, L., Lonsdale, C.J., Lu, R.-S., Mao, J., Marchili, N., Markoff, S., Marrone, D.P., Marscher, A.P., Martí-Vidal, I., Matsushita, S., Matthews, L.D., Medeiros, L., Menten, K.M., Michalik, D., Mizuno, I., Mizuno, Y., Moran, J.M., Moriyama, K., Moscibrodzka, M., Müller, C., Mus, A., Musoke, G., Myserlis, I., Nadolski, A., Nagai, H., Nagar, N.M., Nakamura, M., Narayan, R., Narayanan, G., Natarajan, I., Nathanail, A., Fuentes, S.N., Neilsen, J., Neri, R., Ni, C., Noutsos, A., Nowak, M.A., Oh, J., Okino, H., Olivares, H., Ortiz-León, G.N., Oyama, T., Özel, F., Palumbo, D.C.M., Paraschos, G.F., Park, J., Parsons, H., Patel, N., Pen, U.-L., Pesce, D.W., Piétu, V., Plambeck, R., PopStefanija, A., Porth, O., Pötzl, F.M., Prather, B., Preciado-López, J.A., Psaltis, D., Pu, H.-Y., Ramakrishnan, V., Rao, R., Rawlings, M.G., Raymond, A.W., Rezzolla, L., Ricarte, A., Ripperda, B., Roelofs, F., Rogers, A., Ros, E., Romero-Cañizales, C., Roshanineshat, A., Rottmann, H., Roy, A.L., Ruiz, I., Ruszczyk, C., Rygl, K.L.J., Sánchez, S., Sánchez-Argüelles, D., Sánchez-Portal, M., Sasada, M., Satapathy, K., Savolainen, T., Schloerb, F.P., Schonfeld, J., Schuster, K.-F., Shao, L., Shen, Z., Small, D., Sohn, B.W., Soohoo, J., Souccar, K., Sun, H., Tazaki, F., Tetarenko, A.J., Tiede, P., Tilanus, R.P.J., Titus, M., Torne, P., Traianou, E., Trent, T., Trippe, S., Turk, M., van Bemmell, I., van Langevelde, H.J., van Rossum, D.R., Vos, J., Wagner, J., Ward-Thompson, D., Wardle, J., Weintraub, J., Wex, N., Wharton, R., Wielgus, M., Wiik, K., Witzel, G., Wondrak, M.F., Wong, G.N., Wu, Q., Yamaguchi, P., Yoon, D., Young, A., Young, K., Younsi, Z., Yuan, F., Yuan, Y.-F., Zensus, J.A., Zhang, S., Zhao, G.-Y., Zhao, S.-S., Agurto, C., Allardi, A., Amestica, R., Araneda, J.P., Arriagada, O., Berghuis, J.L., Bertarini, A., Berthold, R., Blanchard, J., Brown, K., Cárdenas, M., Cantzler, M., Caro, P., Castillo-Domínguez, E., Chan, T.L., Chang, C.-C., Chang, D.O., Chang, S.-H., Chang, S.-C., Chen, C.-C., Chilson, R., Chuter, T.C., Ciechanowicz, M., Colin-Beltran, E., Coulson, I.M., Crowley, J., Degenaar, N., Dornbusch, S., Durán, C.A., Everett, W.B., Faber, A., Forster, K., Fuchs, M.M., Gale, D.M., Geertsema, G., González, E., Graham, D., Gueth, F., Halverson, N.W., Han, C.-C., Han, K.-C., Hasegawa, Y., Hernández-Rebollar, J.L., Herrera, C., Herrero-Illana, R., Heyminck, S., Hirota, A., Hoge, J., Hostler

- Schimpf, S.R., Howie, R.E., Huang, Y.-D., Jiang, H., Jinchi, H., John, D., Kimura, K., Klein, T., Kubo, D., Kuroda, J., Kwon, C., Lacasse, R., Laing, R., Leitch, E.M., Li, C.-T., Liu, C.-T., Liu, K.-Y., Lin, L.C.-C., Lu, L.-M., Mac-Auliffe, F., Martin-Cocher, P., Matulonis, C., Maute, J.K., Messias, H., Meyer-Zhao, Z., Montaña, A., Montenegro-Montes, F., Montgomerie, W., Moreno Nolasco, M.E., Muders, D., Nishioka, H., Norton, T.J., Nystrom, G., Ogawa, H., Olivares, R., Oshiro, P., Pérez-Beaupuits, J.P., Parra, R., Phillips, N.M., Poirier, M., Pradel, N., Qiu, R., Raffin, P.A., Rahlin, A.S., Ramírez, J., Ressler, S., Reynolds, M., Rodríguez-Montoya, I., Saez-Madain, A.F., Santana, J., Shaw, P., Shirkey, L.E., Silva, K.M., Snow, W., Sousa, D., Sridharan, T.K., Stahm, W., Stark, A.A., Test, J., Torstensson, K., Venegas, P., Walther, C., Wei, T.-S., White, C., Wieching, G., Wijnands, R., Wouterloot, J.G.A., Yu, C.-Y., Yu, W., Zeballos, M.: First Sagittarius A* Event Horizon Telescope Results. I. The Shadow of the Supermassive Black Hole in the Center of the Milky Way. *Astrophysical Journal Letters* **930**(2), 12 (2022). <https://doi.org/10.3847/2041-8213/ac6674>
- [10] Ponti, G., George, E., Scaringi, S., Zhang, S., Jin, C., Dexter, J., Terrier, R., Clavel, M., Degenaar, N., Eisenhauer, F., Genzel, R., Gillessen, S., Goldwurm, A., Habibi, M., Haggard, D., Hailey, C., Harrison, F., Merloni, A., Mori, K., Nandra, K., Ott, T., Pfuhl, O., Plewa, P.M., Waisberg, I.: A powerful flare from Sgr A* confirms the synchrotron nature of the X-ray emission. *Monthly Notices of the Royal Astronomical Society* **468**(2), 2447–2468 (2017) <https://arxiv.org/abs/1703.03410> [astro-ph.HE]. <https://doi.org/10.1093/mnras/stx596>
- [11] Murakami, H., Koyama, K., Maeda, Y., Sakano, M., Nishiuchi, M., Tsujimoto, M.: Observation of Fe-line Emission from Sagittarius B2 - Evidence for Past Activities of our Galaxy. *Advances in Space Research* **25**(3-4), 579–582 (2000). [https://doi.org/10.1016/S0273-1177\(99\)00804-2](https://doi.org/10.1016/S0273-1177(99)00804-2)
- [12] Revnivtsev, M.G., Churazov, E.M., Sazonov, S.Y., Sunyaev, R.A., Lutovinov, A.A., Gilfanov, M.R., Vikhlinin, A.A., Shtykovsky, P.E., Pavlinsky, M.N.: Hard X-ray view of the past activity of Sgr A* in a natural Compton mirror. *Astronomy and Astrophysics* **425**, 49–52 (2004) <https://arxiv.org/abs/astro-ph/0408190> [astro-ph]. <https://doi.org/10.1051/0004-6361:200400064>
- [13] Ponti, G., Terrier, R., Goldwurm, A., Belanger, G., Trap, G.: Discovery of a Superluminal Fe K Echo at the Galactic Center: The Glorious Past of Sgr A* Preserved by Molecular Clouds. *Astrophysical Journal* **714**(1), 732–747 (2010) <https://arxiv.org/abs/1003.2001> [astro-ph.HE]. <https://doi.org/10.1088/0004-637X/714/1/732>
- [14] Churazov, E., Khabibullin, I., Sunyaev, R., Ponti, G.: Not that long

- time ago in the nearest galaxy: 3D slice of molecular gas revealed by a 110 yr old flare of Sgr A*. *Monthly Notices of the Royal Astronomical Society* **465**(1), 45–53 (2017) <https://arxiv.org/abs/1610.06699> [astro-ph.HE]. <https://doi.org/10.1093/mnras/stw2750>
- [15] Marin, F., Karas, V., Kunneriath, D., Muleri, F.: Prospects of 3D mapping of the Galactic Centre clouds with X-ray polarimetry. *Monthly Notices of the Royal Astronomical Society* **441**(4), 3170–3176 (2014) <https://arxiv.org/abs/1405.0898> [astro-ph.GA]. <https://doi.org/10.1093/mnras/stu741>
- [16] Marin, F., Muleri, F., Soffitta, P., Karas, V., Kunneriath, D.: Reflection nebulae in the Galactic center: soft X-ray imaging polarimetry. *Astronomy and Astrophysics* **576**, 19 (2015) <https://arxiv.org/abs/1502.04894> [astro-ph.GA]. <https://doi.org/10.1051/0004-6361/201425341>
- [17] Ptak, A.: Low-luminosity AGN and normal galaxies. In: White, N.E., Malaguti, G., Palumbo, G.G.C. (eds.) *X-ray Astronomy: Stellar Endpoints, AGN, and the Diffuse X-ray Background*. American Institute of Physics Conference Series, vol. 599, pp. 326–335 (2001). <https://doi.org/10.1063/1.1434645>
- [18] Halderson, E.L., Moran, E.C., Filippenko, A.V., Ho, L.C.: The Soft X-Ray Properties of Nearby Low-Luminosity Active Galactic Nuclei and their Contribution to the Cosmic X-Ray Background. *Astronomical Journal* **122**(2), 637–652 (2001) <https://arxiv.org/abs/astro-ph/0105069> [astro-ph]. <https://doi.org/10.1086/321158>
- [19] Weisskopf, M.C., Soffitta, P., Baldini, L., Ramsey, B.D., O’Dell, S.L., Romani, R.W., Matt, G., Deinger, W.D., Baumgartner, W.H., Bellazzini, R., Costa, E., Kolodziejczak, J.J., Latronico, L., Marshall, H.L., Muleri, F., Bongiorno, S.D., Tennant, A., Bucciantini, N., Dovciak, M., Marin, F., Marscher, A., Poutanen, J., Slane, P., Turolla, R., Kalinowski, W., Di Marco, A., Fabiani, S., Minuti, M., La Monaca, F., Pinchera, M., Rankin, J., Sgro’, C., Trois, A., Xie, F., Alexander, C., Allen, D.Z., Amici, F., Andersen, J., Antonelli, A., Antoniak, S., Attinà, P., Barbanera, M., Bachetti, M., Baggett, R.M., Bladt, J., Brez, A., Bonino, R., Boree, C., Borotto, F., Breeding, S., Brienza, D., Bygott, H.K., Caporale, C., Cardelli, C., Carpentiero, R., Castellano, S., Castronuovo, M., Cavalli, L., Cavazzuti, E., Ceccanti, M., Centrone, M., Citraro, S., D’Amico, F., D’Alba, E., Di Gesu, L., Del Monte, E., Dietz, K.L., Di Lalla, N., Persio, G.D., Dolan, D., Donnarumma, I., Evangelista, Y., Ferrant, K., Ferrazzoli, R., Ferrie, M., Footdale, J., Forsyth, B., Foster, M., Garelick, B., Gunji, S., Gurnee, E., Head, M., Hibbard, G., Johnson, S., Kelly, E., Kilaru, K., Lefevre, C., Roy, S.L., Loffredo, P., Lorenzi, P., Lucchesi, L., Maddox, T., Magazzu, G., Maldera, S., Manfreda, A., Mangraviti, E.,

- Marengo, M., Marrocchesi, A., Massaro, F., Mauger, D., McCracken, J., McEachen, M., Mize, R., Mereu, P., Mitchell, S., Mitsuishi, I., Morbidini, A., Mosti, F., Nasimi, H., Negri, B., Negro, M., Nguyen, T., Nitschke, I., Nuti, A., Onizuka, M., Oppedisano, C., Orsini, L., Osborne, D., Pacheco, R., Paggi, A., Painter, W., Pavelitz, S.D., Pentz, C., Piazzolla, R., Perri, M., Pesce-Rollins, M., Peterson, C., Pilia, M., Profeti, A., Puccetti, S., Ranganathan, J., Ratheesh, A., Reedy, L., Root, N., Rubini, A., Ruswick, S., Sanchez, J., Sarra, P., Santoli, F., Scalise, E., Sciortino, A., Schroeder, C., Seek, T., Sosdian, K., Spandre, G., Speegle, C.O., Tamagawa, T., Tardiola, M., Tobia, A., Thomas, N.E., Valerie, R., Vimercati, M., Walden, A.L., Weddendorf, B., Wedmore, J., Welch, D., Zanetti, D., Zanetti, F.: The Imaging X-Ray Polarimetry Explorer (IXPE): Pre-Launch. *Journal of Astronomical Telescopes, Instruments, and Systems* **8**(2), 026002 (2022) <https://arxiv.org/abs/2112.01269> [astro-ph.IM]. <https://doi.org/10.1117/1.JATIS.8.2.026002>
- [20] Khabibullin, I., Churazov, E., Sunyaev, R.: SRG/eROSITA view of X-ray reflection in the Central Molecular Zone: a snapshot in September–October 2019. *Monthly Notices of the Royal Astronomical Society* **509**(4), 6068–6076 (2022) <https://arxiv.org/abs/2111.07899> [astro-ph.HE]. <https://doi.org/10.1093/mnras/stab3333>
- [21] Revnivtsev, M., Sazonov, S., Churazov, E., Forman, W., Vikhlinin, A., Sunyaev, R.: Discrete sources as the origin of the Galactic X-ray ridge emission. *Nature* **458**(7242), 1142–1144 (2009) <https://arxiv.org/abs/0904.4649> [astro-ph.GA]. <https://doi.org/10.1038/nature07946>
- [22] Di Gesu, L., Ferrazzoli, R., Donnarumma, I., Soffitta, P., Costa, E., Muleri, F., Pesce-Rollins, M., Marin, F.: Prospects for IXPE and eXTP polarimetric archaeology of the reflection nebulae in the Galactic center. *Astronomy and Astrophysics* **643**, 52 (2020) <https://arxiv.org/abs/2008.07830> [astro-ph.HE]. <https://doi.org/10.1051/0004-6361/202037886>
- [23] Ferrazzoli, R., Di Gesu, L., Donnarumma, I., Soffitta, P., Costa, E., Muleri, F., Pesce-Rollins, M., Marin, F.: Prospects for a polarimetric mapping of the Sgr A molecular cloud complex with IXPE. *Astronomy and Astrophysics* **655**, 108 (2021) <https://arxiv.org/abs/2109.06678> [astro-ph.GA]. <https://doi.org/10.1051/0004-6361/202141482>
- [24] Wang, Q.D., Lu, F., Lang, C.C.: X-Ray Thread G0.13-0.11: A Pulsar Wind Nebula? *Astrophysical Journal* **581**(2), 1148–1153 (2002) <https://arxiv.org/abs/astro-ph/0208371> [astro-ph]. <https://doi.org/10.1086/344401>
- [25] Churazov, E., Khabibullin, I., Ponti, G., Sunyaev, R.: Polarization and long-term variability of Sgr A* X-ray echo. *Monthly Notices of the Royal*

- Astronomical Society **468**(1), 165–179 (2017) <https://arxiv.org/abs/1612.00180> [astro-ph.HE]. <https://doi.org/10.1093/mnras/stx443>
- [26] Ferrazzoli, R., Muleri, F., Lefevre, C., Morbidini, A., Amici, F., Brienza, D., Costa, E., Del Monte, E., Di Marco, A., Di Persio, G., Donnarumma, I., Fabiani, S., La Monaca, F., Loffredo, P., Maiolo, L., Maita, F., Piazzolla, R., Ramsey, B., Rankin, J., Ratheesh, A., Rubini, A., Sarra, P., Soffitta, P., Tobia, A., Xie, F.: In-flight calibration system of imaging x-ray polarimetry explorer. *Journal of Astronomical Telescopes, Instruments, and Systems* **6**, 048002 (2020) <https://arxiv.org/abs/2010.14185> [astro-ph.IM]. <https://doi.org/10.1117/1.JATIS.6.4.048002>
- [27] Sunyaev, R., Churazov, E.: Equivalent width, shape and proper motion of the iron fluorescent line emission from molecular clouds as an indicator of the illuminating source X-ray flux history. *Monthly Notices of the Royal Astronomical Society* **297**(4), 1279–1291 (1998) <https://arxiv.org/abs/astro-ph/9805038> [astro-ph]. <https://doi.org/10.1046/j.1365-8711.1998.01684.x>
- [28] Yamauchi, S., Maeda, Y., Koyama, K.: ASCA observation of the Galactic Center. *Advances in Space Research* **19**(1), 63–70 (1997). [https://doi.org/10.1016/S0273-1177\(97\)00038-0](https://doi.org/10.1016/S0273-1177(97)00038-0)
- [29] Churazov, E., Khabibullin, I., Sunyaev, R., Ponti, G.: Can Sgr A* flares reveal the molecular gas density PDF? *Monthly Notices of the Royal Astronomical Society* **471**(3), 3293–3304 (2017) <https://arxiv.org/abs/1705.05878> [astro-ph.HE]. <https://doi.org/10.1093/mnras/stx1855>
- [30] Soderberg, A., Grindlay, J.E., Bloom, J.S., Gezari, S., Piro, A.L., Belloni, T., Liu, J., Berger, E., Coppi, P., Kawai, N., Gehrels, N., Metzger, B., Allen, B., Barret, D., Bazzano, A., Bignami, G., Caraveo, P., Corbel, S., De Luca, A., Fabbiano, P., Finger, M., Feroci, M., Hartmann, D., Hong, J., Jernigan, G., Kaaret, P., Kouveliotou, C., Kutrev, A., Loeb, A., Paizis, A., Pareschi, G., Skinner, G., Di Stefano, R., Tagliaferri, G., Ubertini, P., van der Klis, M., Wilson-Hodge, C.A.: The Dynamic X-ray Sky of the Local Universe. In: *Astro2010: The Astronomy and Astrophysics Decadal Survey*, vol. 2010, p. 278 (2009)
- [31] Rankin, J., Muleri, F., Tennant, A.F., Bachetti, M., Costa, E., Marco, A.D., Fabiani, S., La Monaca, F., Soffitta, P., Tobia, A., Trois, A., Xie, F., Baldini, L., Di Lalla, N., Manfreda, A., O'Dell, S.L., Perri, M., Puccetti, S., Ramsey, B.D., Sgrò, C., Weisskopf, M.C.: An Algorithm to Calibrate and Correct the Response to Unpolarized Radiation of the X-Ray Polarimeter Onboard IXPE. *Astronomical Journal* **163**(2), 39 (2022) <https://arxiv.org/abs/2111.14867> [astro-ph.IM]. <https://doi.org/10.3847/1538-3881/ac397f>

- [32] Kislat, F., Clark, B., Beilicke, M., Krawczynski, H.: Analyzing the data from X-ray polarimeters with Stokes parameters. *Astroparticle Physics* **68**, 45–51 (2015) <https://arxiv.org/abs/1409.6214> [astro-ph.IM]. <https://doi.org/10.1016/j.astropartphys.2015.02.007>
- [33] Di Marco, A., Ratheesh, A., Ferrazzoli, R., La Monaca, F., Rankin, J., Costa, E., Fabiani, S., Muleri, F., Soffitta, P., F., X.: The ixpe x-ray observatory background. In preparation (2021)
- [34] Baldini, L., Bucciantini, N., Lalla, N.D., Ehler, S., Manfreda, A., Negro, M., Omodei, N., Pesce-Rollins, M., Sgrò, C., Silvestri, S.: ixpeobssim: A simulation and analysis framework for the imaging X-ray polarimetry explorer. *SoftwareX* **19**, 101194 (2022) <https://arxiv.org/abs/2203.06384> [astro-ph.IM]. <https://doi.org/10.1016/j.softx.2022.101194>
- [35] Muleri, F., Soffitta, P., Baldini, L., Bellazzini, R., Brez, A., Costa, E., Di Lalla, N., Del Monte, E., Evangelista, Y., Latronico, L., Manfreda, A., Minuti, M., Pesce-Rollins, M., Pinchera, M., Rubini, A., Sgrò, C., Spada, F., Spandre, G.: Performance of the Gas Pixel Detector: an x-ray imaging polarimeter for upcoming missions of astrophysics. In: den Herder, J.-W.A., Takahashi, T., Bautz, M. (eds.) *Space Telescopes and Instrumentation 2016: Ultraviolet to Gamma Ray*. Society of Photo-Optical Instrumentation Engineers (SPIE) Conference Series, vol. 9905, p. 99054 (2016). <https://doi.org/10.1117/12.2233206>
- [36] Vikhlinin, A., Burenin, R.A., Ebeling, H., Forman, W.R., Hornstrup, A., Jones, C., Kravtsov, A.V., Murray, S.S., Nagai, D., Quintana, H., Voevodkin, A.: Chandra Cluster Cosmology Project. II. Samples and X-Ray Data Reduction. *Astrophysical Journal* **692**(2), 1033–1059 (2009) <https://arxiv.org/abs/0805.2207> [astro-ph]. <https://doi.org/10.1088/0004-637X/692/2/1033>
- [37] Sidoli, L., Mereghetti, S.: The X-ray diffuse emission from the Galactic Center. *Astronomy and Astrophysics* **349**, 49–52 (1999) <https://arxiv.org/abs/astro-ph/9908164> [astro-ph]
- [38] Kapteyn, J.C.: On the motion of Nebulae in vicinity of Nova Persei. *Popular Astronomy* **10**, 124–127 (1902)
- [39] Chuard, D., Terrier, R., Goldwurm, A., Clavel, M., Soldi, S., Morris, M.R., Ponti, G., Walls, M., Chernyakova, M.: Glimpses of the past activity of Sgr A* inferred from X-ray echoes in Sgr C. *Astronomy and Astrophysics* **610**, 34 (2018) <https://arxiv.org/abs/1712.02678> [astro-ph.HE]. <https://doi.org/10.1051/0004-6361/201731864>

Methods

IXPE data reduction

The IXPE observatory, as described in detail in [19], includes three identical X-ray telescopes, each comprising an X-ray mirror module assembly (provided by NASA) and a polarization-sensitive Gas Pixel Detector (GPD, provided by the Italian side of the collaboration), to offer spatially resolved X-ray polarimetry in the 2–8 keV energy band. At the Science Operations Center (SOC, at the NASA Marshall Space Flight Center), a software pipeline developed jointly by ASI and NASA processes the relevant science, engineering and ancillary data, estimates the photoelectron emission direction (and hence the polarization), position, and energy of each event after applying corrections for charging effects of the Gas Electron Multiplier (GEM), detector temperature, and gain non-uniformity. The use of the IXPE on-board calibration sources [26] allows correction for time-and-spatially-dependant gain variations of the detectors. The in-flight calibration measurements provide the best knowledge of the gain of the detectors at the time of the observation, and hence the correct energy of each photon, needed to correct the Stokes parameters for the presence of spurious polarization, and to use the correct value of the modulation factor (the modulation amplitude for a 100% linearly polarized radiation [19]). The removal of spurious polarization is achieved using the algorithm of [31].

The output of this pipeline processing is an event file in FITS format for each of the three IXPE detector units that, in addition to the typical information related to spatially resolved X-ray astronomy, contains the event-by-event Stokes parameters [see 32] from which the polarization of the radiation can be derived. The data products are archived at the High-Energy Astrophysics Science Archive Research Center (HEASARC, at the NASA Goddard Space Flight Center), for use by the international astrophysics community. These level-2 event files were cleaned from additional environmental and background contamination [33].

In the case of the observation of the Galactic center, the observation window corresponded to a period of increased solar activity which led to an increase of atmospheric noise (particle background). In addition, such activity tends to extend the South Atlantic Anomaly (SAA), above which the detectors are usually turned off to prevent observation in a highly particle polluted environment. However, as can be seen on Fig. 5 (top), several spikes were recorded in the light-curve right before the spacecraft entry in the SAA. Using the v26.0.0 ixpeobssim tool¹ [34], we removed the count spikes associated with Earth occultation periods and above the extended SAA. Some spurious events attributed to geomagnetic storm events were also flagged and excised. New good time intervals (GTIs) were then computed using these prolonged epochs

¹<https://ixpeobssim.readthedocs.io/en/latest/>

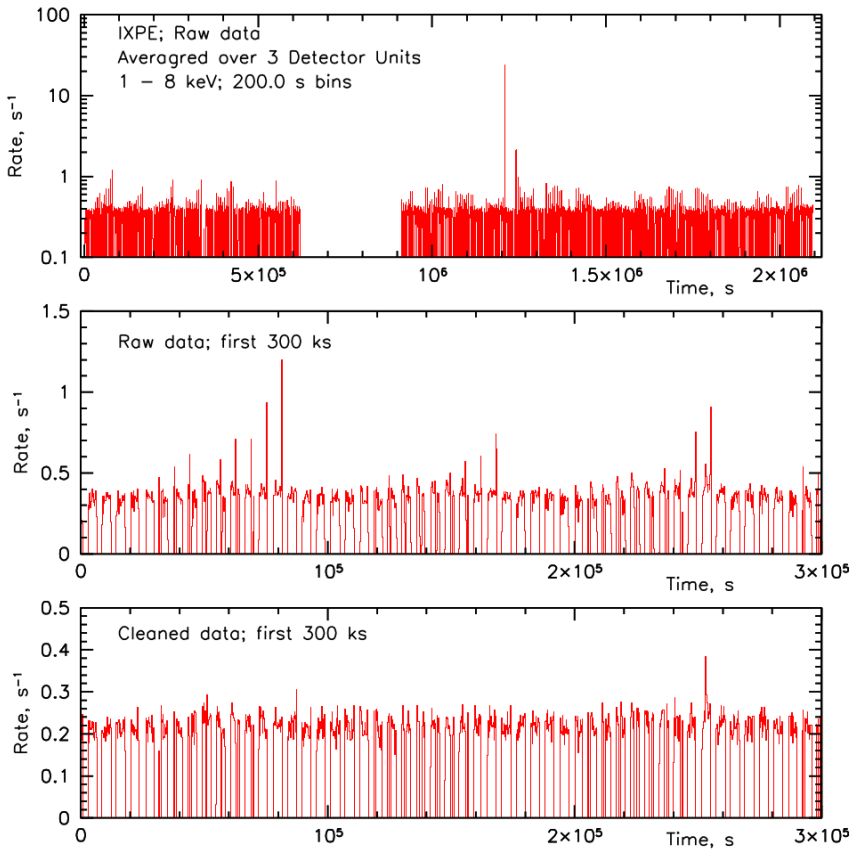


Fig. 5 Illustration of the data cleaning prior to the imaging and spectral analysis. The top panel shows the count rate in the 2–8 keV band (sum of three DUs, 200 seconds time bins) in the original data set that spans 2 million seconds. The two most intense spikes are associated with a geomagnetic storm. To illustrate less prominent variations, the middle panel shows a 300 kiloseconds-long portion of the same light curve that feature a number of smaller amplitude quasi-regular spikes (notice that the vertical scale has changed) that are mostly due to the South Atlantic Anomaly. The gaps in the light curves correspond to moments when the Galactic center was obscured by the Earth. Finally, the bottom panel shows the count rate for the data cleaned from spikes and individual events that most plausibly are due to detector background rather than X-ray photons. The overall count rate in the cleaned data is almost a factor of two lower than in the original data.

and allowed event filtering based on the presence of unaccounted atmospheric noise. After GTI correction (Fig. 5, bottom), the livetime (or Total Good Time) is 0.93 Ms, which represent 96.7% of the livetime before filtering.

IXPE systematic effects

All systematic errors are well below the levels observed from the 4.5' extraction circle we used in this paper. Below, we give a brief statement on each of the

sources of potential systematic effects and refer to the pre-launch papers for a deeper analysis [33, 35]:

- **Instrumental and extra-galactic backgrounds.** From the stacking of almost 2 million seconds worth of background-rejected data from annular background regions around extra-galactic point sources (see Table 1, we also excluded sources bright enough to pollute the background extraction region with their signal because of the wing of the point-spread-function), the background is unpolarized down to a minimum detectable polarization of 3.7% at 99% confidence level. This is well below the measured polarization from the Sgr A region presented in this work.
- **Spurious polarization.** The spurious polarization we managed to calibrate in a 4.5' radius amounts for 0.05%. The statistical error on the derived polarization measurement is 11% (or about 4% modulation). As a consequence, the residual systematic polarization has no effect on the results presented in this paper.
- **Stray light.** The IXPE requirement on the level of stray light is that its suppression should be larger than a factor of 200 (verified at 2.3 keV). We re-scaled the suppression coefficient of the three more intense sources outside the 4.5' radius circle used in this paper as found in the Chandra catalogue (see Tab. 2). The resulting stray-light counting rate (0.5–7 keV) from these sources outside the field of view are 10 μ Crab at most (Crab 0.5–7 keV = 2.8×10^{-8} erg s⁻¹ cm⁻²). Assuming that these sources are 10% polarized, the effect on the observed counting rate is at most 0.1%, i.e. negligible.
- **Solar Effects.** Due to the thick shielding of the detectors, only in case of a very bright X Class solar flare a few photons have been detected (cross-matched by monitoring satellites). Data in coincidence of solar flares are simply removed. In addition, spikes due to passages over the SAA were also removed, as stated previously, and thus do not contribute to systematic effects.
- **Effects related to Earth atmosphere.** The Earth atmosphere, during most of observations, crosses the field of view of IXPE at each orbit. The data are excluded from the analysis. In any case, the atmosphere is dark in the range of IXPE and becomes bright above 10 keV. So we can state that the albedo of Earth is never directly observed by IXPE telescopes. Indirectly, namely through scattering, it contributes to the instrumental background. We can also exclude that any radiation reflected from the atmosphere falls within the field of view of IXPE. In fact the satellite orbits the Earth with an angular velocity of 360° in 90 minutes, which is 4° per minute. This means that the source is seen on the limb of the Earth only within 13', which is 3 seconds each orbit.

Chandra data reduction

The Chandra data reduction follows a standard procedure based on the latest versions of the data reduction software (CIAO v. 4.14) and calibration

Table 1 Observations used in this work for background extraction.

Mission	Obs.ID	Start date (YYYY-MM-DD)	Effective exposure (kiloseconds)	Notes
IXPE	1003701	2022-05-04	96.7	Mrk421
IXPE	1003801	2022-06-04	96.0	Mrk421
IXPE	1004501	2022-03-08	100.4	Mrk501
IXPE	1004701	2022-07-09	97.8	Mrk501
IXPE	1006301	2022-05-06	390.9	BL Lac
IXPE	1006301	2022-05-06	116.9	BL Lac
IXPE	1003501	2022-07-12	771.8	Circinus
IXPE	1005701	2022-06-12	264.2	3C279

Source	Flux	Angular sep. (°)	Suppression factor	Re-scaled flux
2CXO J174621.1-284343	5.033E-11	0.22	245	1.4E-13
2CXO J174451.6-292042	3.949E-11	0.52	752	3.4E-14
2CXO J174445.4-295045	3.387E-11	0.964	1120	2.0E-14

Table 2 The three more intense sources and their re-scaled flux in the extraction region we used in our paper (see Fig. 1). Fluxes are in $\text{erg s}^{-1} \text{cm}^{-2}$.

(CALDB v. 4.9.8). Our particular approach and analysis steps are described in detail in [36]. Briefly, they include identification and removal of high background periods, correction of photon energies for the time and detector temperature dependence of the charge transfer inefficiency and gain, and creation of matching background datasets using blank sky observations with exposure times similar to the Galactic Center pointings.

The Chandra observing program included multiple pointings with individual exposures 10–30 kiloseconds. Due to the spacecraft orientation relative to the Sun, many observations were done with the ACIS focal plane temperature significantly higher than a nominal value of -120 C, resulting in potential problems with the detector gain and response calibration. To minimize the impact of this issue, we have used three Chandra pointings (OBSIDs 24373, 24820, and 26353) with the lowest focal plane temperatures ($T < -116.5$ C) and that were done quasi-simultaneously with the IXPE observations (February 26 through March 11), with a total exposure of 52 kiloseconds.

For the analysis presented here, we use the combined flat-fielded and background-subtracted Chandra image in the 4–8 keV band, and spectra extracted in $4.5'$ circular region discussed above. Following the standard approach for analysing Chandra spectra of extended sources, we have generated the spectral response files that combine the position-dependent ACIS calibration with the weights proportional to the observed brightness in the 4–8 keV band. The extracted spectral data and response files are fit to a set of models as described below.

To assess the impact of the calibration uncertainties associated with the elevated focal plane temperature, we repeated all analyses using the OBSIDs with higher temperatures than the three pointings used in this work. These experiments have shown that after the standard temperature-dependent corrections implemented in CIAO, the parameters of interest for this work (e.g.,

the 4–8 keV flux of the reflected component) are almost unchanged. Therefore, we conclude that the impact of elevated focal plane temperatures on our analysis is negligible.

Archival observations with XMM-Newton

In order to better constrain spectral de-composition of the X-ray emission from the region of interest, we have used all archival observations with XMM-Newton observatory accumulated between 2002 and 2012. These data have already been used for studies of the reflection component [25]. The XMM-Newton data were prepared, reduced and processed in exactly the same manner. As the final step, the spectrum was extracted from the same region as used by IXPE. Thanks to large effective area above 4 keV and long total exposure time supplemented with superior spectral resolution around 6 keV, the XMM-Newton data allow us to better separate thermal and reflected components. Since only the contribution of the reflected component is expected to vary over time, one can combine the archival data with the quasi-simultaneous Chandra and IXPE observations by allowing only parameters of the reflected component model to vary while linking parameters of all other components when fitting the spectra of the total emission observed by all three observatories.

Combined analysis of IXPE, Chandra, and XMM-Newton data

As the first step of the joint IXPE, Chandra and XMM-Newton analysis, the background-subtracted spectra extracted from the circular region shown in Fig. 1 have been fitted with the same multi-component model. This model includes a reflection component and three “thermal” components (an illustrative example of the spectral model is shown in Fig. 6). The latter components can be approximated as emission of optically thin thermal plasma, even though they might now be indeed associated with diffuse X-ray emitting gas. Indeed, in the 4–8 keV energy band, the most important is the thermal component with temperature $kT \sim 6$ keV, which is plausibly due to cumulative emission of large number of point sources, mostly accreting white dwarfs and stars with active coronae [21]. The APEC model² was used for the optically thin thermal components. The reflection component describes the spectrum emerging from a spherical cloud of molecular gas, illuminated by a beam of X-rays, having a power-law spectrum. For this purpose, a publicly available CREFL16 model [25] was used, and more specifically a version of it where reflected continuum and fluorescent lines are treated separately but with tied parameters. A combination of all components provides a reasonably good approximation of the IXPE, Chandra, and archival XMM-Newton spectra

²<http://www.atomdb.org/>

extracted from the reference region³. We note in passing that IXPE and Chandra observations are quasi-simultaneous, while the XMM-Newton data were averaged over several observations spread over many years (from 2002 to 2012). For that reason, the normalization of the reflected component in the XMM-Newton model was decoupled from the IXPE and Chandra models. All other components/parameters were tied across all three instruments.

The outcome of this decomposition procedure was the normalization of the reflected component (expressed in units of surface brightness) and the parameters of the best-fitting CREFL16 model, which do not affect significantly the results of the IXPE data analysis. In principle, some part of the emission with the reflection-like spectrum might be background or foreground with respect to the cloud of interest here, but given the brightness of the selected region compared to the nearby regions, this correction must be subdominant. Critically assessing the spectral decomposition, we concluded that a systematic uncertainty of order 30% is associated with the derived normalization of the reflected component. Since only the scattered continuum of the reflected component is polarized (ignoring second order effects caused by multiple scatterings, [6, 15]), it was singled out and used to fit Q and U spectra measured by IXPE as shown in Fig. 3. For that fit, the scattered continuum component was multiplied by the effective area appropriate for the extraction region (taking into account vignetting) and the modulation factor. For Q and U spectra, the dependence on the polarization angle ϕ was accounted for by introducing multiplicative factors $\cos 2\phi$ and $\sin 2\phi$ in front of the scattered continuum component, for Q and U, respectively. This model is valid in the single scattering approximation.

Sgr A* flare parameters

More than a century ago, Kapteyn [38] realized that for a flare of a compact source and an arbitrary observer, its scattered light with a given time delay since the moment of the flare is associated with the matter located on the surface of an ellipsoid of rotation. The source and the observer are at the foci of the ellipsoid. Furthermore, in close vicinity of the source, the ellipsoid can be approximated by a paraboloid. Assuming that Sgr A* is the primary source, a detection of the scattered light from a cloud relates the age of the flare and the position of the cloud as

$$T = \frac{\sqrt{x^2 + z^2}}{c} + \frac{z}{c}, \quad (1)$$

where c is the speed of light and x and z are the distances of the cloud from Sgr A* in the sky plane and along the line of sight, respectively.

³XSPEC version 12.10.1f was used for fitting the spectra of Chandra, XMM-Newton, and IXPE. For IXPE, XSPEC was also used to fit the Q and U spectra too.

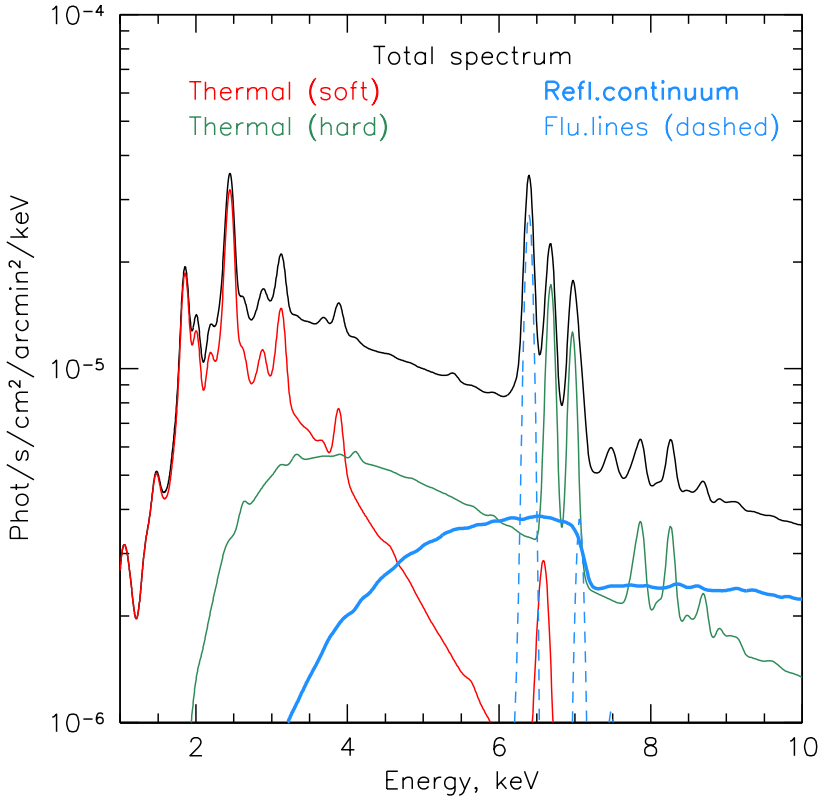


Fig. 6 An illustration of the spectral model used to approximate X-ray spectra extracted from the reference region. For clarity, only two “thermal” components are shown in the plot. The red and the green curves are those thermal components, detailed in [22, 37]. The hotter (green) of the models, having prominent lines at 6.7 and 6.97 keV, contributes significantly to the 4–8 keV band. The blue curves show the two components of the reflected emission. Namely, the dashed blue curves show the fluorescent lines of iron ($K\alpha$ line at 6.4 keV and $K\beta$ line at 7.06 keV), while the thick blue line shows the scattered continuum. Only the latter component is polarized and used to fit the Q and U spectra measured by IXPE. The black line shows the sum of all components. The spectra were convolved with a Gaussian for display purpose.

The degree of polarization P depends on the cosine of the scattering angle μ , which is

$$\mu = -\frac{z}{\sqrt{x^2 + z^2}}. \quad (2)$$

Thus, knowing P , one can reconstruct the 3D position of illuminated clouds. For instance, for $x = 25$ pc and $\theta = 137^\circ$, $z \approx 26$ pc, i.e. the illuminated clouds are further away from us than Sgr A* by this distance.

The determination of the flare luminosity is notoriously difficult, since it depends not only on the distance of the cloud from Sgr A*, but also on the density of the cloud gas and the duration of the flare. One can partly circumvent this problem by using the maximal possible albedo of a molecular cloud [25] to convert the observed X-ray surface brightness into a lower limit on the luminosity

$$L_{4-8,\min} = \frac{I_{4-8}}{\eta_{\max}} 4\pi D_{\text{sc}}^2 \approx 8 \times 10^{37} \text{ erg s}^{-1}, \quad (3)$$

where $I_{4-8} = 4.6 \times 10^{-13} \text{ erg s}^{-1} \text{ cm}^{-2} \text{ arcmin}^{-2} = 5.4 \times 10^{-6} \text{ erg s}^{-1} \text{ cm}^{-2} \text{ sr}^{-1}$ is the observed flux from the studied region [20], $\eta_{\max} \approx 10^{-2}$ is the maximal albedo, and $D_{\text{sc}} = \sqrt{x^2 + z^2} \approx 36$ pc is the distance between Sgr A* and the clouds. Conversion of $L_{4-8,\min}$ to a broader 1–100 keV band assuming a power-law spectrum with the photon index of 2.0 (the value typically measured for the Sgr A GMCs [13]), yields $L_{1-100,\min} \approx 6 \times 10^{38} \text{ erg s}^{-1}$. If the optical depth or, equivalently, the hydrogen column density of illuminated clouds is known, one can use the real albedo in the above equation, driving the minimum luminosity up. Similarly, if only a fraction of the area of the studied region is covered by illuminated clouds, the true luminosity will be higher. For instance, focusing on individual bright clouds, drives this estimate up by an order of magnitude to the level of a few $10^{39} \text{ erg s}^{-1}$ [25] and this is still a lower limit.

However, there is no easy way of placing an upper limit on the source luminosity (for a short flare) without additional explicit assumptions on the gas density and the duration of the flare. For instance, an hour-long flare with a luminosity of $\sim 10^{44} \text{ erg s}^{-1}$ could be consistent with the data.

Finally, we note that the above derivation assumes that all visible reflection emission is due to a single flare. If Sgr A* produced multiple flares over the past several hundred years [4, 39] then the fluxes and polarization will be affected. Longer IXPE observations should be able to test this scenario by providing a polarization measurement of individual GMCs.